Applied Mathematical Modelling 37 (2013) 50–61

Contents lists available at SciVerse ScienceDirect

Applied Mathematical Modelling

journal homepage: www.elsevier.com/locate/apm

Toward design and fabrication of wind-driven vehicles: Procedure to optimize the threshold of driving forces

Parham A. Mirzaei [a,*], Manouchehr Rad [b]

[a] Department of Building, Civil and Environment Engineering, Concordia University, Montreal, Quebec, Canada
[b] School of Mechanical Engineering, Sharif University of Technology, Azadi st., Tehran, Iran

ARTICLE INFO

Article history:
Received 9 April 2011
Received in revised form 2 November 2011
Accepted 13 November 2011
Available online 20 November 2011

Keywords:
Land-yacht
Aerodynamics
Airfoil
CFD
Wind energy

ABSTRACT

Wind energy has been continuously considered as a green, available, and economical alternative source of energy. For centuries, the transformed wind energy to drag-force has been used for transportation in watercrafts. With improvement of aerodynamics, the airfoil was invented to create and use a higher magnitude aerodynamic force, lift-force, in order to elevate airplanes. Later, the lift-force was horizontally applied as the thrust force in land/water wind-crafts. Whereas in airplanes horizontal airfoils (wing) create a vertical lift-force, installed vertical airfoils (wing-sail) produce a horizontal lift-force in wind-crafts. Therefore, this force can be used as thrust (driving) force in lift-based ice, water, and land vehicles. If the prevailing wind is constantly available, the vehicle speed can even exceed the wind velocity. Due to the complex kinematics of such vehicles, however, it should be noted that there would be always an optimum for the thrust force in order to control and navigate the vehicle to the destination point, and to avoid the severe undesired side-forces. This optimum is calculated in wind-craft trajectory software (WTS) which requires many inputs, including variable and constant parameters. Variable parameters consist of wind direction and magnitude in addition to vehicle's position, velocities, and accelerations. On the other hand, design characteristics of the wind-driven vehicle are known as constant parameters. The land-yacht body's drag is an unknown constant parameter which alters according to the relative wind. This implies that several wind tunnel experiment in different wind directions and speeds are required in order to obtain the drag coefficients.

Therefore in order to bypass the wind tunnel measurements, this study aims to propose a fast and economical procedure to find the aforementioned drag coefficient by integration of a measurement and by a simulation approach. The obtained data can be later used in the optimization and control module of the WTS. The performance of this procedure has been investigated using a case study. For this purpose, a 1:4 prototype three-wheel land-yacht is first designed and fabricated. The land-yacht comprises of three major parts; horizontal airfoil (axle), vertical airfoil, and body. The dimensions of these elements are obtained after development of a code based on kinematics of the land-yacht. The axle is designed to increase the stability of the land-yacht, whereas the shape of the body is intended to produce a low drag coefficient in various directions. Furthermore, a set of experiments has been conducted to measure the body drag of the land-yacht in a direction parallel to the relative wind. This experiment is later used to develop and validate a computational fluid dynamics (CFD) model in order to estimate the drag of the land-yacht body in its various directions against the relative wind. The results show the adequate efficacy of this procedure to provide the required data for the optimization and control module of the WTS.

* Corresponding author.
E-mail address: p_mirzae@encs.concordia.ca (P.A. Mirzaei).

0307-904X/$ - see front matter © 2012 Published by Elsevier Inc.
doi:10.1016/j.apm.2011.11.037

Nomenclature

x, y, z	Cartesian axis (m)
$\dot{x}, \dot{y}$	velocity in x and y directions (m s^{-1})
$\ddot{x}, \ddot{y}$	acceleration in x and y directions (m s^{-2})
M	weight of the land-yacht (kg)
$A_P, \dot{A}_p, A_{\lambda-\alpha}$	effective area of the vertical and horizontal airfoils, and land-yacht body due to its direction (m^2)
N_i ($i = 1,2,3$)	normal forces to the wheels (N)
F_{fx}, F_{fy}	friction force of wheels in x and y directions (N)
F_{Dx}, F_{Dy}	drag-force of the land-yacht body in x and y directions (N)
F_L, F_D	total lift and drag-force on the vertical airfoil (N)
F_{Down}	downward lift-force on the horizontal airfoil (N)
$C_{L(\alpha,Re)}$, $C_{D(\alpha,Re)}$	lift and drag coefficients on the vertical airfoil
$C_{L(Re)}$	lift coefficient on the horizontal airfoil
$C_{D(\lambda-\alpha,Re)}$	drag of the land-yacht body due to its direction
α	angle of attack (°)
β	angle of the land-yacht relative to XY coordinate (°)
λ	angle of the vertical airfoil relative to xy coordinate (°)
ρ	density (kg m^{-3})
μ_x, μ_y	friction coefficient of wheels in x and y directions
$\overline{U}_{rel}$	relative wind velocity vector due to the land-yacht (m s^{-1})
$\overline{U}_{\infty}$	prevailing wind vector (m s^{-1})
H_1, H_2	land-yacht vertical dimensions (m)
D, L, L_2, L_3, L_4	land-yacht horizontal dimensions (m)
Re	Reynolds number $= \frac{\overline{U}_{\infty} l}{\upsilon}$

1. Introduction

Civilization has an indisputable debt to wind energy whose contribution ranges from the development of agriculture to the improvement of human transportation; from ancient windmills to recent wind farms which provide 2% of worldwide electricity energy [1]. Sailing is referred as the first technique to implement wind energy for human transportation beginning from late millenniums [2]. Entering the 20th century, wind energy has been again employed to make a dream come to an end; capturing the sky. This was not possible without improvement of aerodynamics [3,4]. Studies have been revealed that the lift-force has a larger order of magnitude than drag-force. This concept has been referred to a revolution in implementation of the wind energy in aviation industry [5]. On the other hand, effort has been conducted to take the advantage of this green, available, and economical energy in sail and land yachts [6–8]. Thus, the lift-force was produced in the lift-based vehicles using one or several flexible or rigid vertical wing-sails [9–11]. The wing-sails are mostly designed with the shape of an airfoil, and installed on wheels/ship to be used in land/water. Theoretically, the airfoil can constantly produce a lift-force which can cause a higher velocity in the yacht than its prevailing wind. For example, a speed of 203.1 km/h is recorded for a land-yacht on March 26, 2009 when wind speeds were fluctuating between 48 and 80 km/h [12]. The lift-based vehicles are not only useful on Earth, but it is desired to use them in other planets as explorer robots, where the wind energy with high velocity is mostly available and access to solar radiation might be impossible. However, the main drawback of such vehicles in highly fluctuated winds is their complexity in providing a proper angle of attack against the relative wind in order to steer the land-yacht to a planned destination. At the moment, the angle of wing-sail is manually adjusted by land sailors learned through experience. Therefore, to develop persistent wind-driven vehicles, it is necessary to evolve their steering mechanisms from manual to automatic.

As shown in Fig. 1, the wind-craft trajectory software (WTS) is considered to navigate the land-yacht to the desired destination based on variable parameters, including the prevailing wind velocity and direction. Moreover, design parameters are known as constant factors for the WTS. In general, the WTS has two major parts, including kinematics, as well as optimization and control modules which can calculate an optimum angle of attack for the vertical airfoil regarding to the variable and

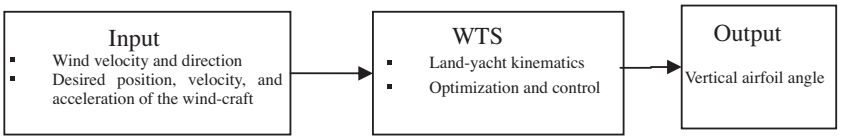

Fig. 1. Diagram of necessary steps to obtain maximum force in desired navigation direction.

constant parameters. While variable parameters can be obtained by installing necessary sensors on the wind-craft, constant variables are mostly provided through design characteristics of a land-yacht. The only unknown parameter is the drag coefficients of land-yacht body which is a function of wind speed and direction. This means that extensive wind-tunnel experiments have to be performed in order to measure this coefficient.

Thus, this study aims to develop a simulation model in order to bypass the wind-tunnel process, and provide appropriate kinematics information for the optimization and control module of the WTS. For this purpose, kinematics of the land-yacht is first developed. Then, a land-yacht prototype is designed and fabricated to guaranty the stability of the land-yacht for velocities up to 20 m/s. This prototype has three major parts: horizontal axle (airfoil), vertical airfoil, and land-yacht body. A set of experiments combined with a computational fluid dynamics (CFD) model is later developed to approximate the only unknown parameter of the land-yacht's trajectory model, the drag coefficient of the land-yacht body. Consequently, the optimization and control module of the WTS will be able to recommend a unique angle for the vertical airfoil in order to provide suitable thrust force to navigate the land-yacht.

2. Kinematics of the land-yacht

To design the land-yacht prototype, it is necessary to first derive the dynamics of a land-yacht [13,14]. As shown in Fig. 2, the studied land-yacht has three wheels. The front wheel has a steer mechanism while a vertical airfoil produces thrust force. The projection of the driving force in moving coordinate (xy) can be derived as below:

$$[F_L \sin(\lambda-\alpha) + F_D \cos(\lambda-\alpha)] - F_{Dx} - F_{fx} = M\ddot{x}, \tag{1}$$

$$[F_L \cos(\lambda-\alpha) - F_D \sin(\lambda-\alpha)] - F_{Dy} - F_{fy} = M\ddot{y}, \tag{2}$$

where M is the weight of the land yacht. F_L and F_D are respectively the airfoil lift and drag forces created by relative wind. Also, F_{Dx} and F_{Dy} represent drag of the land-yacht body in x and y, respectively. α is angle of attack. β and λ denote the angle of the land-yacht and airfoil relative to fixed coordinate (XY) and moving coordinate (xy), respectively. Moreover, F_{fx} and F_{fy} are respectively the friction of wheels in x and y directions. Obviously, F_{fy} shows the side-slip effect of the land-yacht and has larger order of magnitude than F_{fx} which is the rolling friction of the wheels:

$$F_{fx} = F_{f\text{-side1}} + F_{f\text{-side2}} + F_{f\text{-side3}} = (N_1 + N_2 + N_3)\mu_x, \tag{3}$$

$$F_{fy} = (N_1 + N_2 + N_3)\mu_y, \tag{4}$$

$$Mg + F_{Down} - N_1 - N_2 - N_3 = 0, \tag{5}$$

where g is the gravity acceleration. μ_x and μ_y are respectively the friction coefficients of wheels in x and y directions. N_i ($i = 1,2,3$) are the normal forces to the wheels. Obviously, μ_y has a negligible magnitude and can be omitted in calculations. Also, F_{Down} demonstrates the downward lift-force of the horizontal NACA0012 airfoil (see Fig. 3). It is worth mentioning that

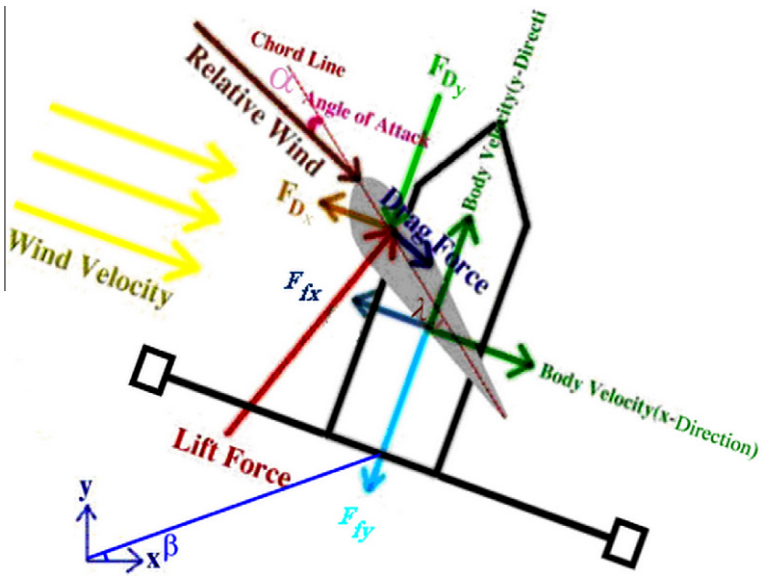

Fig. 2. Diagram of kinematic forces for the land-yacht.

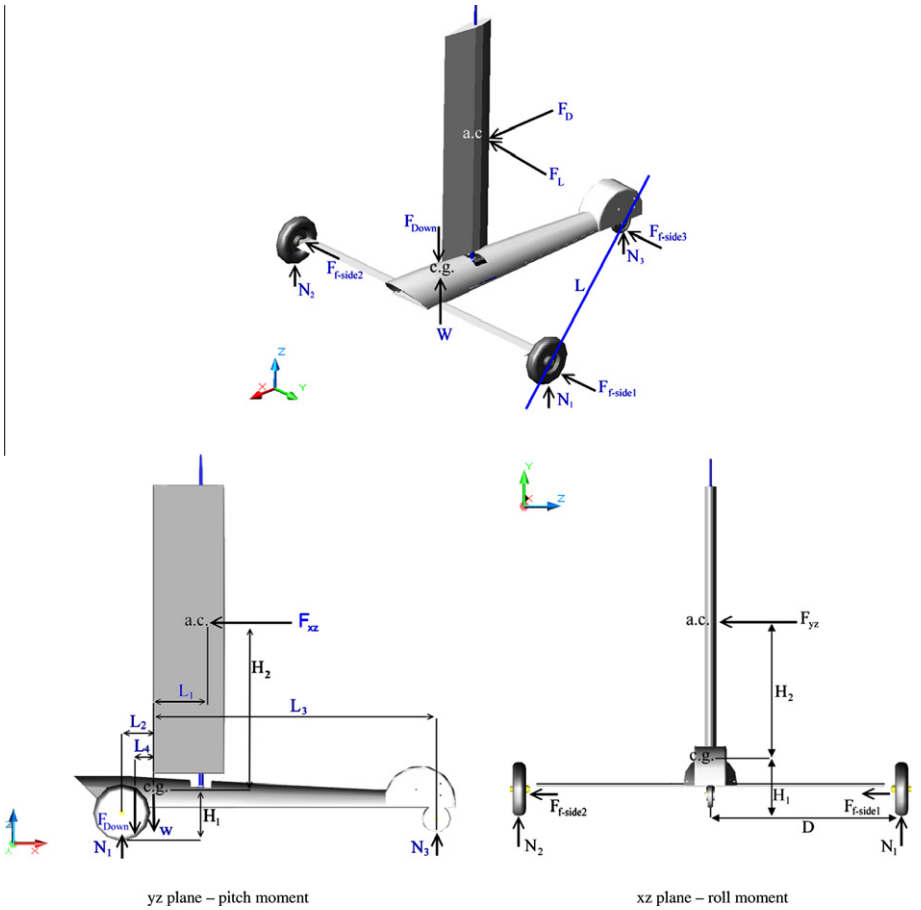

Fig. 3. Moment diagrams of the prototype land-yacht.

the angle of attack for the axle (horizontal airfoil) is designed and fixed to be 3°. One can also calculate the vertical and horizontal airfoil lift and drag forces as follows [3]:

$$F_L = \frac{1}{2}\rho C_{L(\alpha,Re)} A_P U_{rel}^2, \tag{6}$$

$$F_D = \frac{1}{2}\rho C_{D(\alpha,Re)} A_P U_{rel}^2, \tag{7}$$

$$F_{Down} = \frac{1}{2}\rho \dot{C}_{L(Re)} \dot{A}_P U_{rel}^2, \tag{8}$$

where ρ is the air density, and A_P and $\dot{A}_p$ are the effective area of the vertical and horizontal airfoils (the length of airfoil span multiply by its chord length), respectively. $C_{L(\alpha,Re)}$ and $C_{D(\alpha,Re)}$ are respectively the lift and drag coefficients, and depend on α and Reynolds number $\left(Re = \frac{\overline{U}_\infty l}{\upsilon}\right)$. These coefficients are mostly provided for standard types of airfoils (here; NACA0012). However, $\dot{C}_{L(Re)}$ is only a function of Reynolds number since its angle of attack is constant (3°). F_{Dx} and F_{Dy} can be also obtained from the following equations:

$$F_{Dx} = \frac{1}{2}\rho C_{D(\lambda-\alpha,Re)} A_{\lambda-\alpha} U_{rel}^2 \cos(\lambda - \alpha), \tag{9}$$

$$F_{Dy} = \frac{1}{2}\rho C_{D(\lambda-\alpha,Re)} A_{\lambda-\alpha} U_{rel}^2 \sin(\lambda - \alpha), \tag{10}$$

where $C_{D(\lambda-\alpha,Re)}$ is the drag coefficient of the land-yacht body and varies by changing the angle of land-yacht body due to the relative wind. $A_{\lambda-\alpha}$ is also the effective area of land-yacht body due to its direction. This implies that $A_{\lambda-\alpha}$ is the projection of

the land-yacht surface area in each $\lambda-\alpha$ ($A\times\cos(\lambda-\alpha)$ for F_{Dx} and $A\times\sin(\lambda-\alpha)$ for F_{Dy}). The presented procedure in Section 4 demonstrates an approach to find $C_{D(\lambda-\alpha,Re)}$. The relative wind changes continuously with direction of the land-yacht and can be illustrated as below:

$$\overline{U}_{rel}=\overline{U}_{\infty}-(\dot{\bar{x}}^2+\dot{\bar{y}}^2)^{0.5}, \tag{11}$$

where $\overline{U}_{\infty}$ is the prevailing wind vector, and $\overline{U}_{rel}$ is the relative wind velocity vector due to the land-yacht. $\dot{x}$ and $\dot{y}$ are also the land-yacht velocity vectors in x and y direction, respectively.

Moreover, Eqs. (12)–(14) show the forces applied to the aerodynamic center (a.c) and center of gravity (c.g) of the land-yacht. In order to increase the stability of the vehicle in higher velocities, it is important to select appropriate dimensions for the land-yacht (illustrated in Fig. 3). This implies that the parameters should be designed in a conservative range to prevent the rotation of the land-yacht around L-axis. The projections of the moments around the L-axis in the xz and yz planes are known as roll and pitch, respectively. Also, yaw moment explains how the land-yacht spins around z axis in the xy plane (Fig. 2). These moments can be derived as below:

$$\Sigma M_{xz}=[F_L\sin(\lambda-\alpha)+F_D\cos(\lambda-\alpha)]H_2+(N_1-N_2)D\pm\mu_x\{(N_1+N_2+N_3)H_1\}, \tag{12}$$

$$\Sigma M_{yz}=[F_L\cos(\lambda-\alpha)-F_D\sin(\lambda-\alpha)]H_2+F_{Down}L_4-(N_1+N_2)L_2+N_3L_3\mp\mu_y\{(N_1+N_2+N_3)H_1\}, \tag{13}$$

$$\Sigma M_{xy}=[F_L\sin(\lambda-\alpha)+F_D\cos(\lambda-\alpha)]L_1\pm\mu_x\{(N_1+N_2)L_2-N_3L_3\}\pm\mu_y\{(N_1-N_2)\mathrm{D}\}, \tag{14}$$

where ΣM_{xz}, ΣM_{yz}, and ΣM_{xy} represent roll, pitch and yaw moments, respectively. Also, the direction of the friction forces is always employed in opposite direction of the land-yacht movement. It is worth mentioning that c.g. and the pressure center of land-yacht body are designed to be very close to each other; their distance is assumed to be zero in moments' calculations.

In order to find reliable dimensions for parameters, a code is developed to predict the trajectory of the land-yacht based on Eqs. (1)–(14). Knowing the prevailing wind velocity and direction, and fixing the vertical airfoil to gain a maximum lift and drag forces, priority of the developed code is defined to prevent the land-yacht from roll, pitch, and yaw. Thus, the priorities and restrictions applied to the code can be presented as follows:

- Preserve the roll, pitch, and yaw around zero.
- Preserve the side forces around zero.
- Assume a maximum length and width of 1.5 m for the land-yacht prototype.
- Assume a maximum height of 2 m for the land-yacht prototype.
- Preserve a maximum weight of 10 kg for the land-yacht prototype.

The obtained sizes for various parameters of the land-yacht are depicted in Table 1. These numbers guarantee the stability of the designed land-yacht for velocities up to 20 m/s. It is worth mentioning that lift and drag coefficients for standard airfoils (NACA0012), and $A_{\lambda-\alpha}$ are provided a priori for the developed code. However, the drag coefficient of land-yacht body ($C_{D(\lambda-\alpha,Re)}$) is the only approximated parameter. Therefore, a set of experiment-simulation is proposed to find the exact value of this number for the WTS.

3. Fabrication of the land-yacht prototype

As depicted in Fig. 4a, the axle is designed as a horizontal airfoil to conserve the stability of wind-craft in high velocities, to produce a small drag against the relative wind, and to perform a downward lift-force. It should be mentioned that this

Table 1
Calculated parameters of the land-yacht prototype.

Parameter	Value
L_1	17.5 cm
L_2	10.0 cm
L_3	99.1 cm
L_4	8.8 cm
H_1	16.3 cm
H_2	57.0 cm
D	71.0 cm
W	8 kg
Vertical airfoil height	100.0 cm
Vertical airfoil chord	50.0 cm
Horizontal airfoil height	120.0 cm
Horizontal airfoil chord	10.0 cm

Fig. 4. Different parts of the land-yacht prototype.

lift-force will be produced since the vertical airfoil (NACA0012) is installed with 3° angle of attack. NACA0012 is a broadly recommended and used airfoil in literature due its symmetrical shape and proper characteristics against the stalling [15]. The horizontal airfoil is fabricated from aluminum alloy 7020 [16]. The chord and span lengths are also presented in Table 1.

Fig. 4b demonstrates the vertical NACA0012 airfoil required to produce driving forces. The 00-series airfoil provides a reasonable lift coefficient and stall angle. In order to avoid unnecessary moments, the center of moments needs to be projected on the aerodynamic center (Fig. 3 and Table 1). Moreover, balsa wood coated with fiberglass strings is selected to fabricate this airfoil.

Eventually, the land-yacht body (shown in Fig. 4c) is designed and fabricated from ABS copolymer to first protect the controlling systems, devices, and servo-motors implemented to rotate the vertical airfoil and front-wheel according to the WTS. Its aerodynamic shape also helps to reduce resisting drag in different angle of the relative wind. This point will be later observed in Fig. 11 where the drag coefficient at various angles is relatively low. To obtain the complex drag-force of the land-yacht body, a procedure using a set of experiments integrated with a CFD simulation is proposed in the next section.

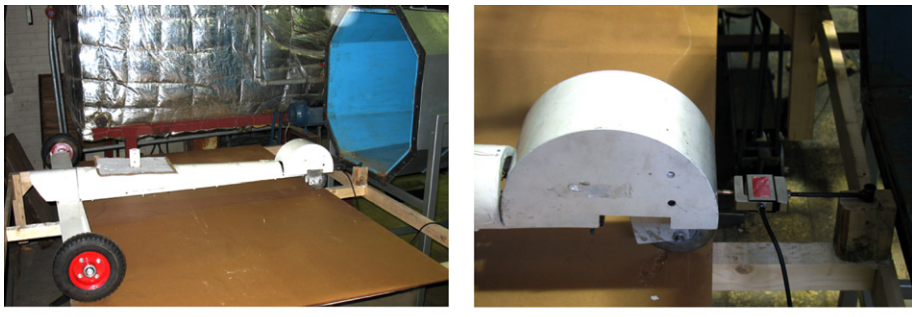

Fig. 5. Land-yacht body drag test.

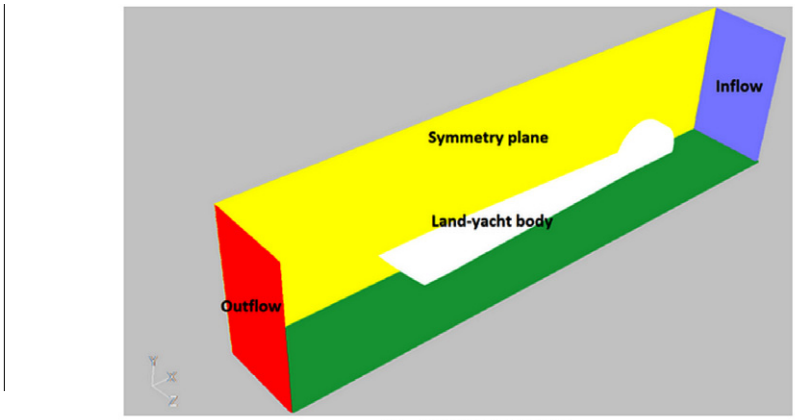

(a) CFD study domaim

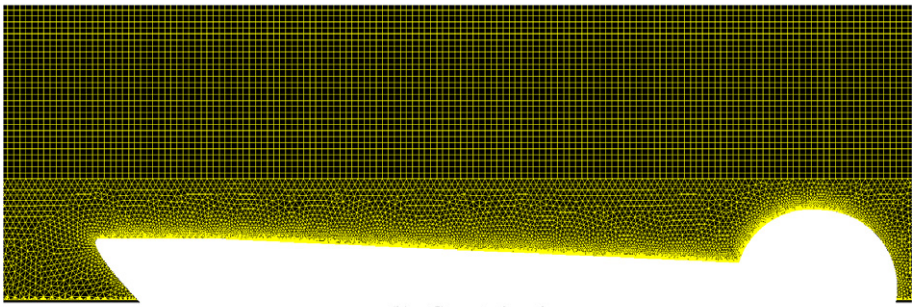

(b) Generated meshes

Fig. 6. Simulation approach to calculate drag coefficient on the land-yacht body.

4. Procedure to find drag of the land-yacht body

To provide data for the optimization and control part of the WTS, all parameters presented in Eqs. (1)–(14) are known except $C_{D(\lambda-\alpha,Re)}$. This drag coefficient, however, cannot be precisely found using analytical techniques. Thus, in this section, a procedure consisting of a measurement and a simulation model is presented to calculate $C_{D(\lambda-\alpha,Re)}$.

4.1. Experiment

First, a set of experiments is developed in order to measure the effect of prevailing wind on the land-yacht body when the relative angle between them is zero ($\lambda - \alpha = 90^\circ$). For this purpose, the airflow with velocities ranging from 2 m/s to 20 m/s

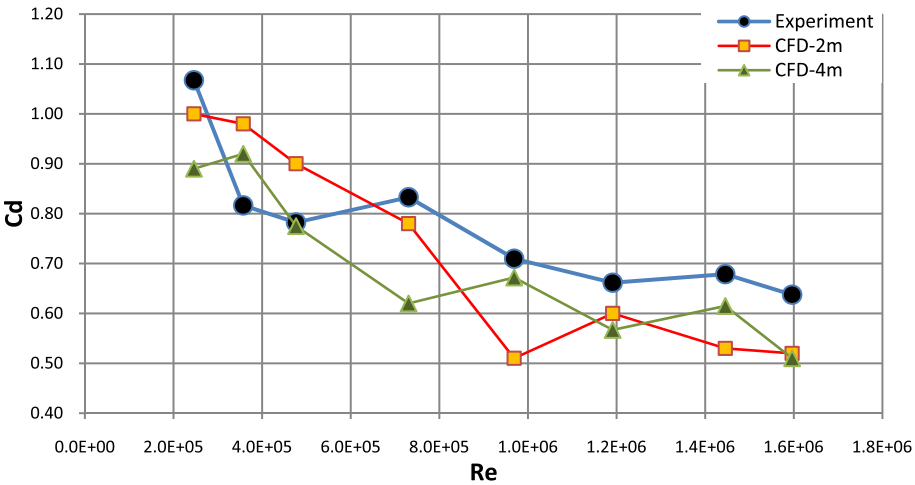

Fig. 7. Measurement and CFD simulation of drag coefficient of the land-yacht body.

is passed over the land-yacht body (Fig. 5a). As depicted in Fig. 5b, an S-type load cell is later installed to record the force according to the drag effect on the land-yacht body. The measured drag coefficients are demonstrated in Fig. 7. The $C_{D(\lambda-\alpha=90^\circ,Re)}$ may be obtained using Eqs. (9) and (10). In the next section, the obtained data are used to validate the simulation model for the prediction of $C_{D(\lambda-\alpha,Re)}$ when $\lambda-\alpha$ is changing. However, here, it is expected that the measurement does not fully represent the real situation of the land-yacht movement. The source of this discrepancy might be attributed to the stationary wheels in the experiment. The rolling friction coefficient between wheels and road is significantly different than the stationary friction coefficient between wheels and the wooden testing board (Fig. 5).

4.2. CFD simulation

One approach to find aforementioned $C_{D(\lambda-\alpha,Re)}$ is to implement computational fluid dynamics (CFD) simulation over the wind-craft body. For this purpose, the airflow is assumed to pass over the wind-craft in different angles. Here, to decrease the number of calculations, only five angles (0°, 45°, 90°, 135° and 180°) are simulated using Fluent [17] software. This implies that the WTS can then interpolate $C_{D(\lambda-\alpha,Re)}$ from simulated angles. A 2 m $\times$ 0.5 m $\times$ 0.5 m ($x \times y \times z$) domain is created in order to model the airflow over the wind-craft (Fig. 6a). The current size for the domain is obtained from a parametric study for three dimensions; x, y, and z. It is observed that the selected sizes for the section of the study domain (yz-plane) are adequate enough to avoid the interference of the walls on flow pattern over the land-yacht body. The length of the study domain

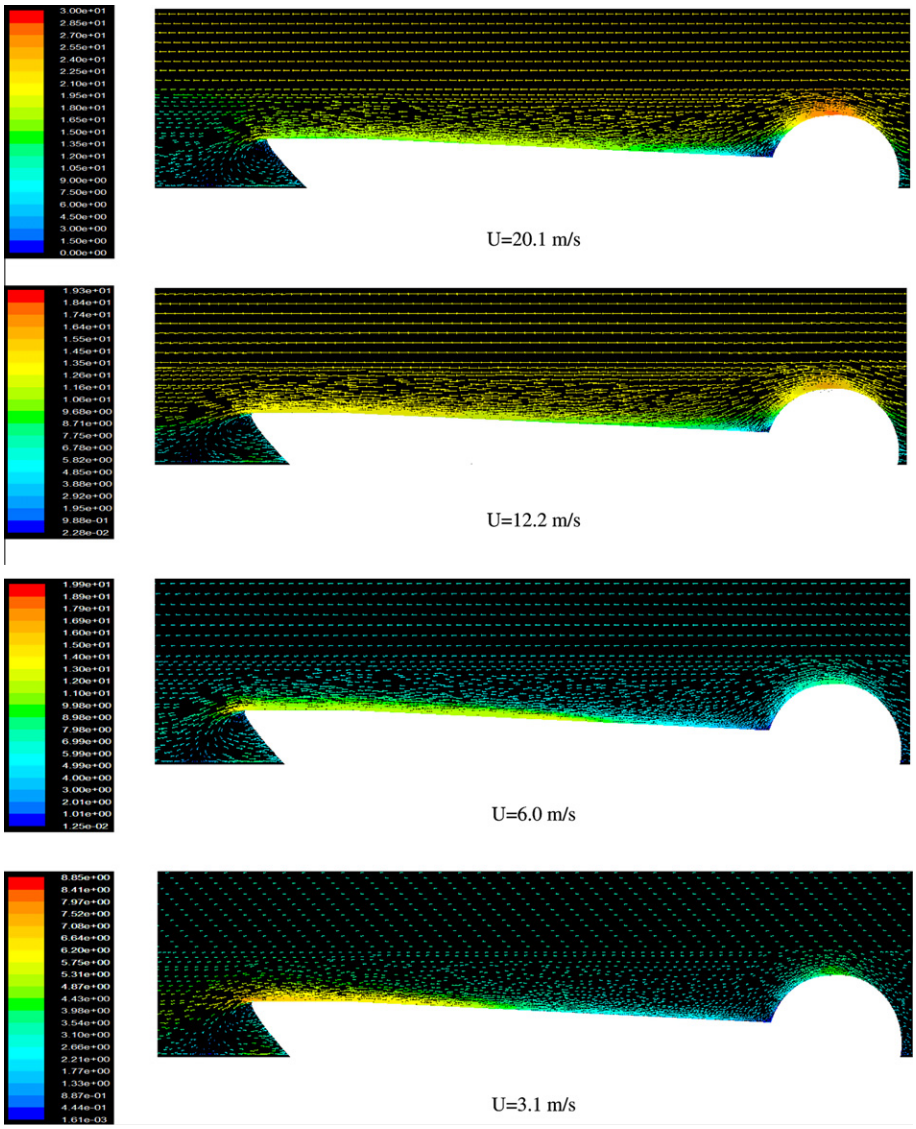

Fig. 8. Airflow pattern over the land-yacht body in different upstream velocities.

(x) however has to be long enough in order to capture the separated flow pattern from the tail of the land-yacht body. It is also necessary to consider a tradeoff between length size and number of generated cells. In Fig. 7, two study domains with length of 2 m (CFD-2 m) and 4 m (CFD-4 m) are compared to the aforementioned experiment in previous section. Therefore, the inflow velocity is changed several times according to the experiment. The domain length less than 2 m engenders an enormous discrepancy while more than a 4 m length does not have a significant effect on the results. As it is shown in Fig. 7, CFD-4 m have lower overall discrepancy (11%) than that of CFD-2 m (14%) although CFD-4 m underestimates the drag coefficient, especially in medium range Reynolds number where the error is about 26%. This number is 6% for CFD-2 m. This implies that a huge advantage cannot be always gained using longer length for the domain size.

Selecting CFD-2 m and for the validation of the airflow model, over 1.1 million tetrahedron/hexahedron cells are generated using Gambit software [18] where the minimum and maximum size of the cells are 1.4^{-10} m^3 and 1.1^{-6} m^3,respectively. The meshes are mostly refined on surfaces of the land-yacht to capture the viscosity within the boundary layer region which significantly affects the formation of the drag-force (Fig. 6b). In validation simulation, half of the domain is also modeled due to the symmetry of the problem. Simulation domain and assigned boundary conditions are also illustrated in Fig. 6a. Moreover, standard K–ε turbulence model is selected with enhanced wall-treatment for surface of the study domain and land-yacht body. Furthermore, second-order upwind is employed as discretization scheme for momentum equation. SIMPLE algorithm is performed as numerical procedure to solve the Navier–Stokes equation.

5. Results and discussion

As shown in Fig. 7, the obtained results demonstrate the capability of the CFD model in calculating the wind-craft body's drag coefficient. The overall and maximum 14% and 21% errors between simulation and experiment are also calculated in this study, respectively. It is noteworthy to mention that there is an uncertainty on a share of calculated discrepancies for the measurement (i.e. device calibration, rolling effect of the wheels) and CFD (i.e. domain size, turbulent scheme, grid size). In general, the CFD model illustrates a suitable accuracy for prediction of the flow pattern over the land-yacht body through different Reynolds numbers.

As expected from theory, the drag coefficient decreases as Reynolds number increases in both simulation and experiment studies shown in Fig. 7. Fig. 8 demonstrates how airflow passes the land-yacht body. According to this figure, it can be concluded that the airflow regime over the body lays mostly in the turbulent region when its pattern does not significantly change with increase of upstream velocity. As it is expected from theory, the airflow first reaches its maximum speed on the top of the half-cylinder (around 120°) where separation occurs (Fig. 8). As mentioned before, the half-cylinder is necessary to protect the steering system. Furthermore, the airflow slips over the sloped shaft of the land-yacht body until it reaches the tail, where the airflow is slightly separated. Here, a weak vortex can be seen below the tail in Fig. 9. As it can be seen from the normalized velocities, in higher upstream velocities the magnitude of the airflow close to the tail significantly reduces as its value (U/U_∞) from U_∞ = 3.1 (m/s) to U_∞ = 20.1 (m/s) varies approximately from 2.5 to 0.75. Obviously,

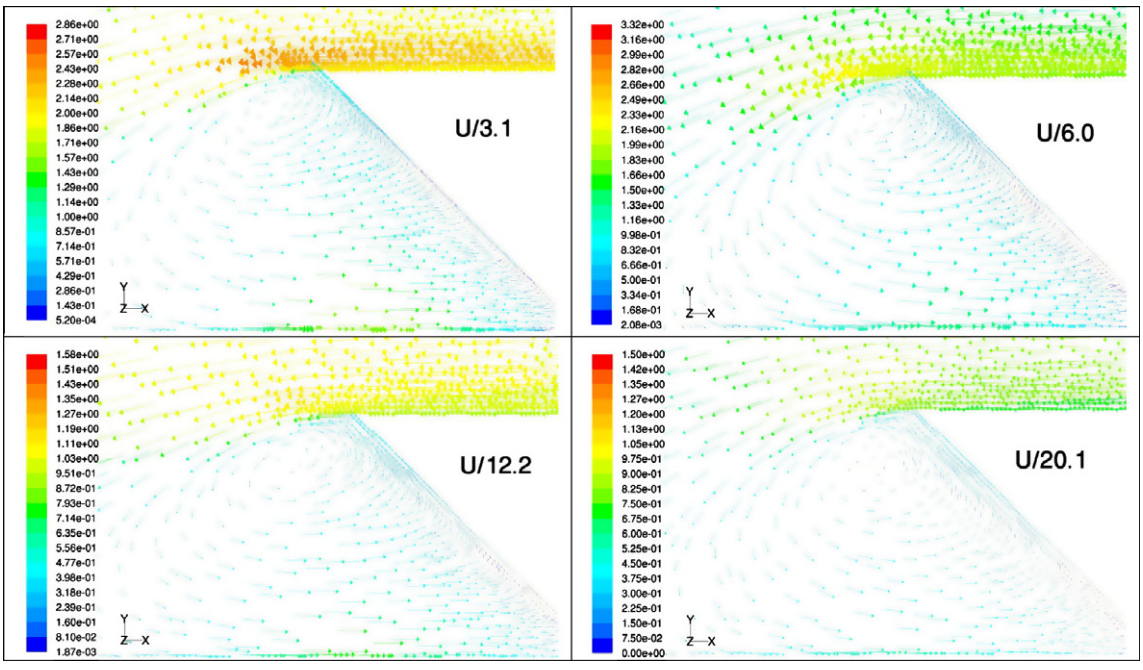

Fig. 9. Normalized airflow pattern on tail of the land-yacht body in different upstream velocities.

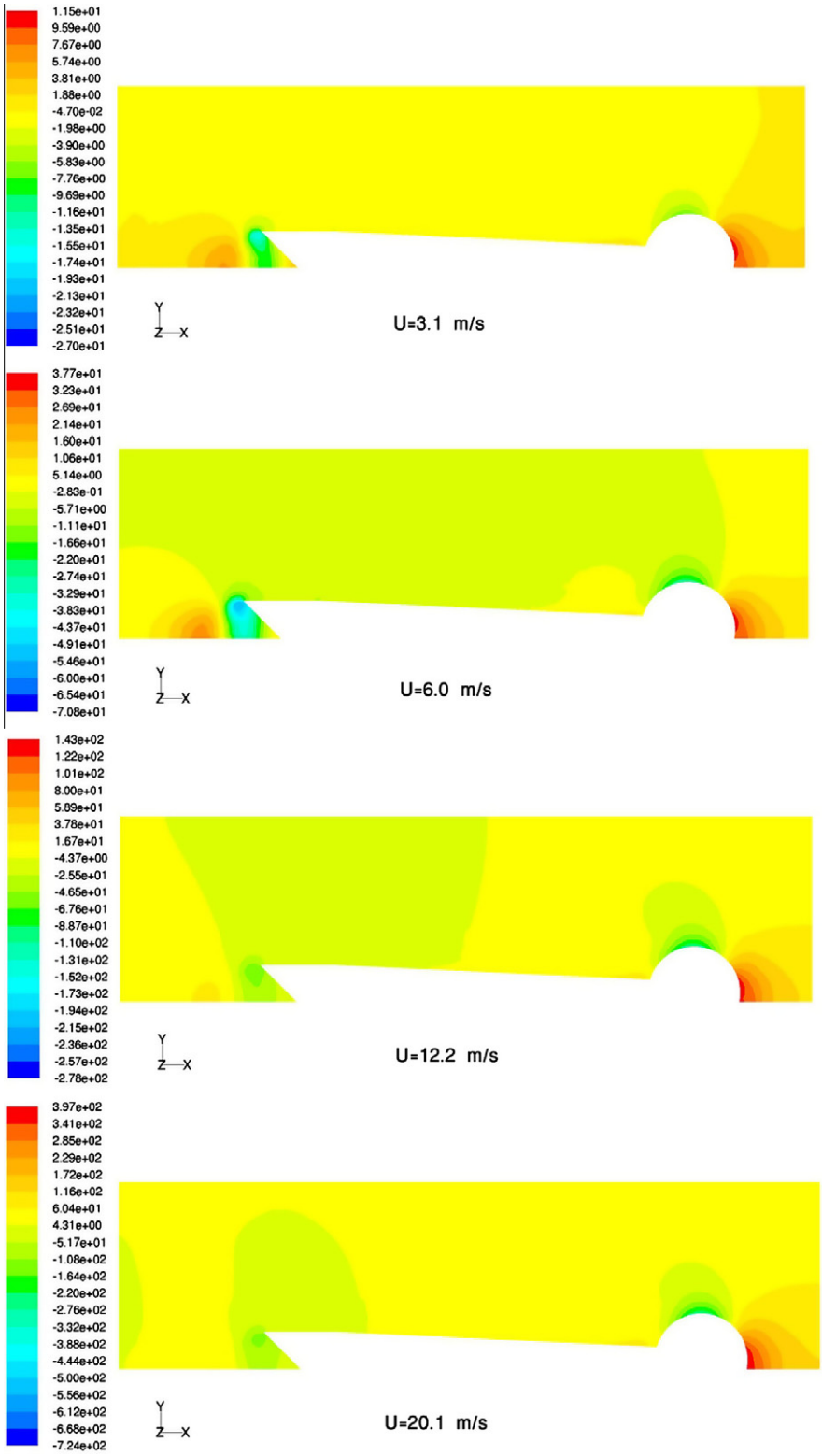

Fig. 10. Pressure contours over the land-yacht body in different upstream velocities.

the separation creates weaker backflow in higher velocities and reduces the drag of the land-yacht body. Furthermore, the pressure contours for velocities 3.1, 6.0, 12.2, and 20.1 (m/s) are depicted in Fig. 10. As expected again, a strong negative pressure field after the tail of the land-yacht vanishes as upstream velocity increases. This shows again the influence of the tail vortex which is deteriorated in the higher Reynolds numbers.

The validated CFD model in the previous section provides an adequate accuracy for further development of a practical prediction tool in order to estimate $C_{D(\lambda-\alpha,Re)}$ which denotes the drag coefficient at various angles of attacks $(\lambda-\alpha)$ and Reynolds numbers.

Because of the symmetry in the shape of the land-yacht body ($C_{D(0^\circ\to180^\circ,Re)} = C_{D(360^\circ\to180^\circ,Re)}$), only drag coefficient in half of the domain, $C_{D(0^\circ\to180^\circ,Re)}$, is calculated. For this purpose, the airflow is discretized with five angles $(\lambda-\alpha)$, including 0°, 45°, 90°, 135°, and 180°. Also, eight velocities are simulated for each angle resulting 40 simulation sets in total (as illustrated in Fig. 11). Obviously, a desired angle existing between two calculated angles can be interpolated to obtain $C_{D(\lambda-\alpha,Re)}$. One can also refine the current 45° interval to smaller sectors for retrieving better resolution.

As expected, drag coefficients decrease independently in each angle with the increase in Reynolds number (Fig. 11). The decrease rate is higher when $\lambda-\alpha=0^\circ$ and lower when $\lambda-\alpha=90^\circ$. When $\lambda-\alpha=180^\circ$, changes in the drag coefficient show the minimum value in both higher and lower Reynolds numbers. For $\lambda-\alpha=45^\circ$ and $\lambda-\alpha=135^\circ$, a same pattern can be almost seen with a high drag coefficient around $C_D=0.8$ in higher Reynolds number while it decreases to about $C_D=0.5$ within lower Reynolds. Fig. 11 acknowledges design efficacy of the land-yacht body since higher drag coefficient are attributed to $\lambda-\alpha=0^\circ$ knowing that the $\lambda-\alpha$ mostly exists around 45° during the land-yacht navigation. The obtained results of this figure can be later integrated to the WTS in order to calculate the threshold of driving forces. It should be again

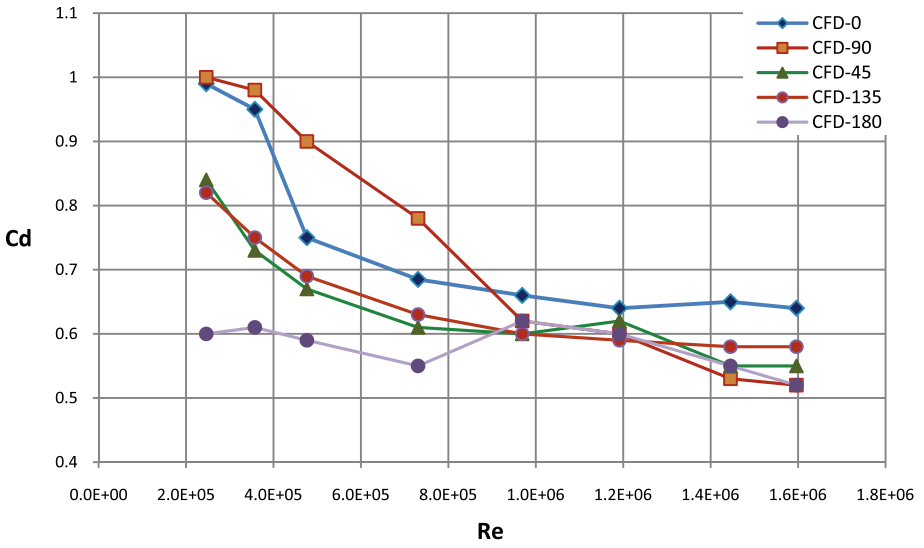

Fig. 11. Drag coefficient of the land-yacht body against the upstream wind with different angles.

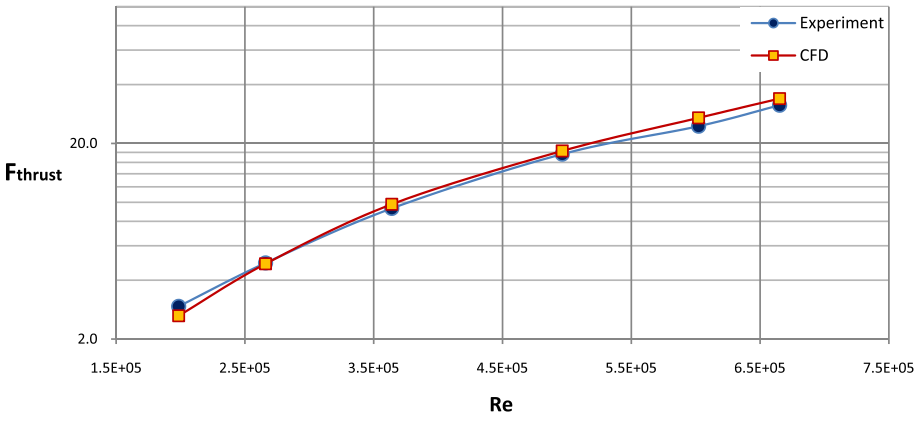

Fig. 12. Thrust force of the land-yacht for $\lambda=0$ and $\alpha=-20$ in different Reynolds numbers.

noted that passing a certain path with efficient speed is a task of the optimization and control part of the WTS using obtained dataset from this part.

To verify the result of Fig. 11, another set of experiments is conducted to assure the performance of the proposed procedure. For this reason, a random angle is selected to test the imposed forces on the land-yacht prototype. Therefore, the whole land-yacht is placed parallel to an upstream relative wind as $\lambda = 0^\circ$ and $\alpha = -20^\circ$ while the total thrust force imposed to the land-yacht in x-direction is measured using an S-type load cell. As illustrated in Fig. 12, the driving force elevates from 3 ($N\,m^{-2}$) to 32 ($N\,m^{-2}$) when the relative wind velocity increases from 3.1 ($m\,s^{-1}$) to 20.1 ($m\,s^{-1}$). In this case, the side forces are not large enough to slide the land-yacht in y-direction (see Figs. 2 and 3).

Using Eq. (2), representing the dynamic of the land-yacht in x-direction, one can calculate the driving force in x-direction as the only unknown parameter is $C_{D(\lambda-\alpha=20^\circ,Re)}$. This value can be extracted and interpolated from Fig. 11. As illustrated in Fig. 12, the predicted driving forces through the prediction model are fairly compatible with measured thrust force where the mean error is about 6%. Similar to the measurement, the calculated thrust force increases as Reynolds number elevates. This means that the land-yacht can have a maximum initial acceleration of 3.9 ($m\,s^{-2}$) when $\overline{U}_{rel} = 20.1\ (m\,s^{-1})$, $\lambda = 0^\circ$ and $\alpha = -20^\circ$. This number is comparable with initial acceleration of modern automobiles.

6. Conclusion

The kinematics of a three-wheel land-yacht is derived followed by a code in order to obtain the required dimension for a 1:4 land-yacht prototype. After the design and fabrication of the land-yacht prototype, an experiment is conducted to measure the drag coefficient of the land-yacht body in various velocities. These numbers are then used to validate a CFD model in order to generate a dataset for imposed driving force over the land-yacht body. This data set is then used in kinematics of the land-yacht to estimate the driving-force. Comparison of the calculated thrust force with another measurement dataset approves the capability of the developed procedure as the average discrepancy between measurement, and CFD is obtained less than 6%. This clearly approves the adequacy of the CFD model in order to provide the required parameter for the optimization and control module of the WTS. This means that the developed procedure can significantly reduce the number of required measurements.

Many innovative and conceptual designs can help to enhance the kinematics of the land-yachts to reach higher accelerations for future investigations. Studies have to be conducted for providing more efficient driving-forces using advancer airfoils as well as mechanism to prevent dissipated energy through the slid motion of the wheels. Moreover, it is also necessary to improve the proposed procedure by development of more accurate CFD models. Furthermore, advanced approaches such as Artificial Neural Network (ANN) and Genetic Algorithm (GA) are potential alternatives for the optimization and control module of the WTS. Eventually, it is possible to integrate other sources of sustainable energy (e.g. solar) to the land-yacht by installing photovoltaic panels on vertical and/or horizontal airfoils.

Acknowledgement

The authors would like to express their gratitude to the Center of Excellence in Energy Conversion (CEEC) of Sharif University of Technology for their financial support.

References

[1] WWEA, The World Wind Energy Report 2009, 2009.
[2] P. Johnstone, The Sea-craft of Prehistory, Routledge, 1980.
[3] J.R. Anderson, Fundamentals of Aerodynamics, McGraw-Hill, New York, 1984.
[4] V.A. Tucker, G.C. Parrott, Aerodynamics of gliding flight in a falcon and other birds, J. Exp. Biol. 52 (1970) 345–367.
[5] I.H. Abbott, A.E. Von Doenhoff, Theory of Wing Sections, Dover, New York, 1959.
[6] C. Ciortan, C. Guedes Soares, Computational study of sail performance in upwind condition, Ocean Eng. 34 (2007) 2198–2206.
[7] R.G.J. Flay, I.J. Vuletich, Development of a wind tunnel test facility for yacht aerodynamic studies, J. Wind Eng. Ind. Aerodyn. 58 (1995) 231–258.
[8] L. Larsson, L. Broberg, K.-J. Kim, D.H. Zhang, A method for resistance and flow prediction in ship design, Tran. Soc. Naval Arch. Mar. Eng. 98 (1990) 495–535.
[9] J.G. Walker, A high performance automatic wing sail auxiliary propulsion system for commercial ships, J. Wind Eng. Ind. Aerodyn. 20-3 (1985) 83–96.
[10] P. Van Oossanen, Predicting the speed of sailing yachts, Trans. Soc. Naval Arch. Mar. Eng. 101 (1993) 337–397.
[11] J. Yoo, H.T. Kim, Computational and experimental study on performance of sails of a yacht, Ocean Eng. 33 (2006) 1322–1342.
[12] NALSA, 2011. <http://www.nalsa.org/index.htm>.
[13] W.H. Hucho, Aerodynamics of Road Vehicles, Butterworth, Boston, 1986.
[14] P.S. Jackson, Modelling the aerodynamics of upwind sails, J. Wind Eng. Ind. Aerodyn. 63 (1996) 17–34.
[15] M. Al-atabi, Aerodynamics of wing tip sails, J. Eng. Sci. Technol. 1 (1) (2006) 89–98.
[16] J.G. Kaufman, Aluminum Alloy Database, Knovel, 2004.
[17] FLUENT, 2008. <http://www.ansys.com/Products/Simulation±Technology/Fluid±Dynamics/ANSYS±FLUENT>.
[18] GAMBIT, 2008. <http://fluent.com/software/gambit/>.